Reset Transition in HfO_2-Based Memristors Using a Constant Power Signal

Héctor García*[a], Guillermo Vinuesa[a], Mireia B. González[b], Francesca Campabadal[b], Helena Castán[a], Salvador Dueñas[a]

[a] *Dpto. Electricidad y Electrónica, Universidad de Valladolid, Paseo de Belén 15, 47011, Valladolid, Spain*

* *Corresponding author. E-mail address: hecgar@ele.uva.es*

[b] *Institut de Microelectrònica de Barcelona, IMB-CNM (CSIC), Carrer dels Til·lers s/n, Campus UAB, 08193, Bellaterra, Spain*

Abstract

Memristors, also known as resistive switching devices, have great potential for applications in memory and neuromorphic systems. Understanding the switching mechanisms is crucial since ReRAM memories need to operate at high frequencies. It is known the reset transition is dominated by the conductive filament Joule heating. We have studied the reset transition in TiN/Ti/HfO_2/W metal–insulator–metal memristors by applying constant power signals to different initial filament thicknesses, which were obtained using different initial low resistance states. The results show that power value controls the reset times, decreasing when the power is increased. On the other hand, larger resistances lead to faster reset transitions These measurements have allowed us to obtain a value of the thermal resistance of the conductive filament. Moreover, we have observed the reset times as a function of the initial resistance and the power lies on a common plane, which allows us to estimate the transition time by fixing an initial resistance and a power value.

Keywords: Memristor, Resistive switching, Reset transition, Hafnium oxide

1. Introduction

Memristors are based on the resistive switching (RS) phenomenon, which has been studied since the 1960s when negative resistance was observed in some binary metal oxides [1]. The RS effect occurs when an electric field is

able to change the resistance of a thin dielectric film between two different values in a non-volatile way: a high resistance value (HRS) and a low resistance value (LRS). Different devices based on the RS effect has been widely studied for several applications, such as digital storage (resistive RAMs or ReRAMs) [2, 3], artificial neurons in neuromorphic systems out of the Von Neumann architecture paradigm [4, 5], logic circuits [6, 7] and cryptographic circuits [3, 8].

Metal-insulator-metal (MIM) capacitors are commonly used as memristors. The formation (set process) and rupture (reset process) of a conductive filament (CF) which can short-circuit the metal electrodes is responsible for the resistance change. In valence-change devices (VCMs), the CF is due to positively charged oxygen vacancies inside the dielectric layer, as a great concentration of oxygen vacancies can lead to a leakage path with metallic properties [9]. One electrode of the MIM capacitor is oxygen affine so it can act as an oxygen reservoir storing oxygen ions during the set transition ad releasing them during the reset transition. Some metals as Ti [10] or Ta [11] are known to be oxygen affine. The other electrode should be inert. This filamentary model is widely accepted by the scientific community [12, 13]. Usually, an initial electroforming process is necessary to create one or several conductive filaments of oxygen vacancies inside the switching layer, which connects the top and bottom electrodes. This electroforming process can determine the size of the initial filaments [14, 15].

A wide variety of materials have been studied as potential candidates for resistive switching devices [16], and metal oxides are promising candidates. Several metal oxides and transition metal oxides (TMO) have demonstrated resistive switching behavior [17, 18, 19, 20]. Among them, hafnium oxide (HfO_2) is a promising material mainly due to its compatibility with the CMOS process and high-density integration [21]. This material is also being studied for emulating synaptic plasticity in neuromorphic systems [22]. Therefore, both dielectric film and metal electrodes play an important role in the switching characteristics of the MIM structures.

Switching times of memristors are of great importance as ReRAMs should be able to work at higher frequencies than conventional DRAMs. However, switching times in $\sim$ 50-100 ns range are found in commercially available memristors, which makes them slower than state-of-the-art DRAM [23]. Moreover, the time response of memristors-based artificial neurons to potentiation and depression pulses is also an important issue [24]. In classical memories (SRAM, DRAM and Flash) the stored information change is due

to variations in the amount of stored electrons. However, the stored information change in ReRAMs is due to variations of an atomic configuration. The ion movement inside the insulator is due of both diffusion and drift mechanisms [25, 26]. As the ionic mass is much higher than the electron mass, the switching time is potentially smaller in conventional memories; however, faster switching memristors (<1 ns) have been reported [23, 27]. Joule heating is present during the set and reset transitions [28, 29], and there are experimental observations of the temperature increase [28, 30]. At timescales above 10 ns, the movement of oxygen vacancies limits the switching speed meanwhile at lower timescales the Joule heating speed of the VCM device and the electrical charging time are also relevant [31]. Anyway, it is not completely clear how fast a redox-based resistive switching device can switch.

In this work, we have measured the switching times for the reset transition using TiN/Ti/HfO_2/W MIM memristors. Instead of applying a constant voltage signal, we have applied a constant power signal. We have used different initial resistance state conditions, so different CF shapes before applying voltage pulses. Using these results, an estimation of the thermal resistance can be obtained.

2. Experimental

TiN/Ti/10nm-HfO_2/W metal-insulator-metal RS devices were used to carry out the electrical measurements. The HfO_2 layer was grown by atomic layer deposition using TDMAH and water as hafnium and oxygen precursors, respectively, at a temperature of 225 °C. The bottom electrode, a 50 nm-thick W layer, was deposited by magnetron sputtering. The top electrode, consisting of a 200 nm-thick TiN layer on a 10 nm-thick Ti layer, was also grown by magnetron sputtering and patterned by a lift-off process. A schematic representation of the RS devices is shown in Fig. 1(a). The resulting structures used in this work are square cells of 40×40 μm^2. The resistive switching behavior of the devices was previously studied, and the conductive filaments were assumed to be due to different oxygen vacancies concentration in the HfO_2 film [32], as physically-based models suggested [33]. Fig. 1(b) shows several current-voltage (I-V) cycles which reveals bipolar resistive switching, where set transition takes place for positive top electrode voltages and reset transition for negative voltages. The inset figure shows a previous electroforming process, which is necessary to obtain the RS behavior. A 10

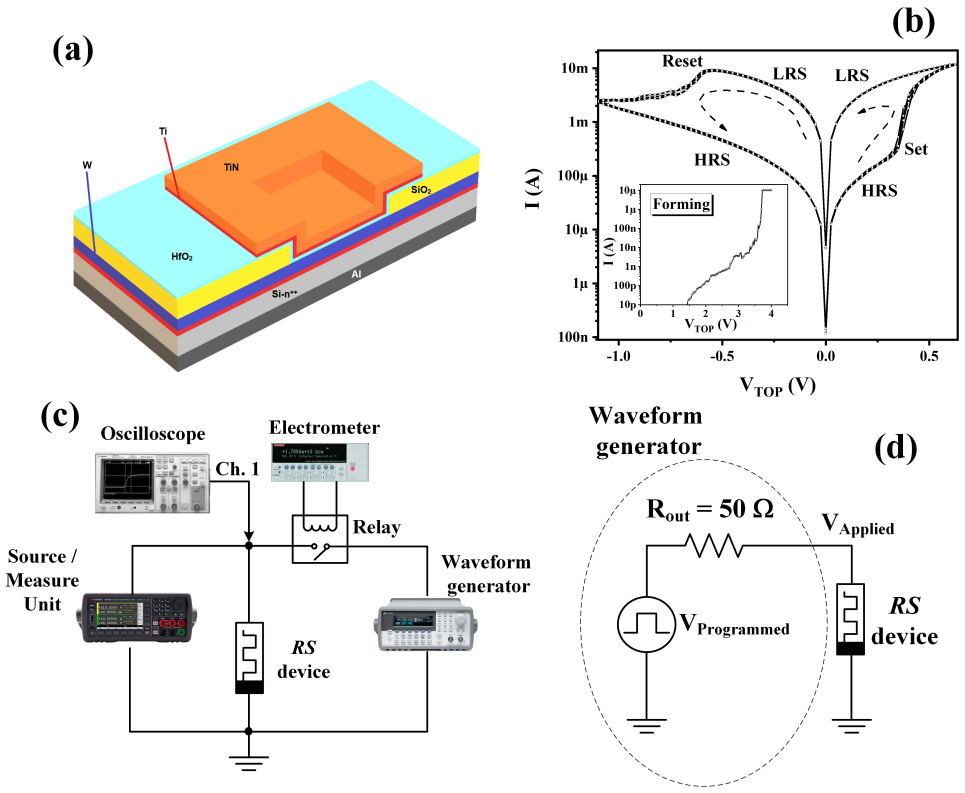

Figure 1: Schematic representation of the RS device (a). Several I-V cycles showing bipolar RS behavior (b) and the electroforming process (inset (b)). Experimental set-up used to measure the voltage transients (c), and equivalent circuit when applying the voltage pulses (d).

μA compliance current was used to avoid irreversible oxide breakdown during the forming process.

In order to carry out the voltage transients, the setup shown in Fig. 1(c) was used. A Keysight B2912B precision source/measure unit was used to initially drive the RS device to the LRS by applying a voltage ramp with an amplitude of +0.8 V, but using three different compliance values: 8, 10, and 12 mA. Once the device is in the LRS, a Keysight 33250A waveform generator applies a voltage pulse ($V_{Programmed}$) which drives the devices to the HRS (reset transition), and the voltage drop across the RS device ($V_{Applied}$) is recorded by an HP54615B oscilloscope. A relay controlled by a Keithley 6517A electrometer is used to disconnect the waveform generator from the RS device when the Keysight B2912B applies the initial voltage ramp. The equivalent circuit when applying the voltage pulses is shown in Fig. 1(d). The voltage drop across the RS device can be calculated as

$$V_{Applied} = V_{Programmed} \cdot \frac{R_{LRS}}{R_{LRS} + 50\Omega} \tag{1}$$

and, as the initial resistance value (R_{LRS}) can be easily obtained because the device is in the LRS (whose resistance is a constant value), the $V_{Programmed}$ value can be obtained for each measurement. The current which flows through the RS device can be calculated as

$$I = \frac{V_{Programmed} - V_{Applied}}{50\Omega} \tag{2}$$

and finally, the resistance value of the device is

$$R = \frac{V_{Applied}}{I} \tag{3}$$

As an example of the measurement procedure, Fig. 2(a) shows the voltage signal as directly obtained from the oscilloscope when the initial current compliance in the set transition was 12 mA, and we programmed a voltage step such $V_{Applied}$ obtained is -0.5 V. The signal is then shifted so the pulse is applied at t=0 s and the signal is also smoothed using an adjacent-average filter (see Fig. 2(b)). We now can obtain the current (not shown here) and the resistance which is shown in Fig. 2(c). The initial resistance in the LRS obtained with the I-V measurement was 54 Ω and is exactly the resistance value obtained at t=0 s. Then, up to a time of about 600 μs, the resistance

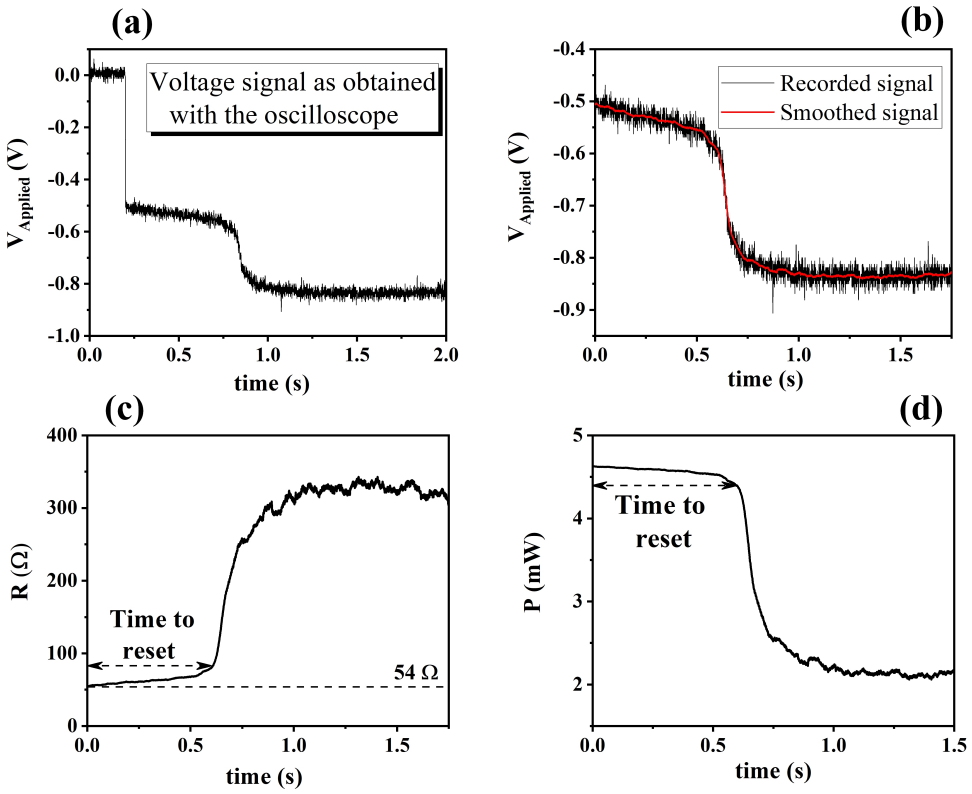

Figure 2: For the reset transition, voltage transient signal as obtained from the oscilloscope (a), voltage transient smoothed (b), resistance transient (c) and power transient (d). Time to reset parameter is shown in (c) and (d).

slightly increases. This corresponds to a filament which is getting thinner as we have also proposed in a previous work where we measured I-V curves for high ramp-rate voltage [34]. Simulation models for similar structures also proposed this behavior [35]. After 600 μs, the resistance suddenly increases, which corresponds to the CF breaking. We have defined the parameter *time to reset* as the time required for the filament to thin enough to start the CF breaking, so, as shown in Fig. 2(c), it is the time required for the resistance to increase abruptly. It is important to note this is a feedback process: once the device resistance increases, $V_{Applied}$ also increases because $V_{Programmed}$ and the waveform generator output resistance remain constant. This feedback process makes it possible to keep the power dissipation constant (the increase in the voltage drop across the device balances the resistance decrease). Fig. 2(d) shows the power dissipated by the device when applying the voltage pulse: the power value can be considered constant until the CF is broken (during the time to reset). The CF rupture results in a sudden power decrease, due to a sudden resistance increase.

3. Results

We achieved different initial resistances in LRS by using different current compliances as shown in Fig. 3(a). In this figure, we can observe several I-V curves when using 8, 10 and 12 mA current compliances. The current in LRS increases when the current compliance increases, giving place to a lower R_{LRS}, as shown in Fig. 3(b), where the resistance value for the different I-V cycles is represented. The devices reached three initial R_{LRS} values: 68, 62 and 54 Ω. These resistance values are constant as long as the device remains in the LRS. Fig. 3(c) shows the power vs. voltage curves. The power value for which the reset is reached increases when the current compliance increases due to a greater CF thickness. As will be discussed below, the reset transition can be achieved at different powers but at different times.

Once the device is in the LRS, an applied voltage step drives the device to the HRS. $V_{applied}$ vs. time is recorded by the oscilloscope. Then, as explained in the experimental section, we can obtain the power dissipated by the device as a function of time. Fig. 4 shows power vs. time curves when the initial R_{LRS}=54 Ω (12 mA current compliance) for different voltage amplitudes, ranging from -0.50 V to -0.85 V. The power dissipated increases as the voltage amplitude increases, giving place to faster reset transitions. The filament dissolution in TMO-based memristors and other metal oxides

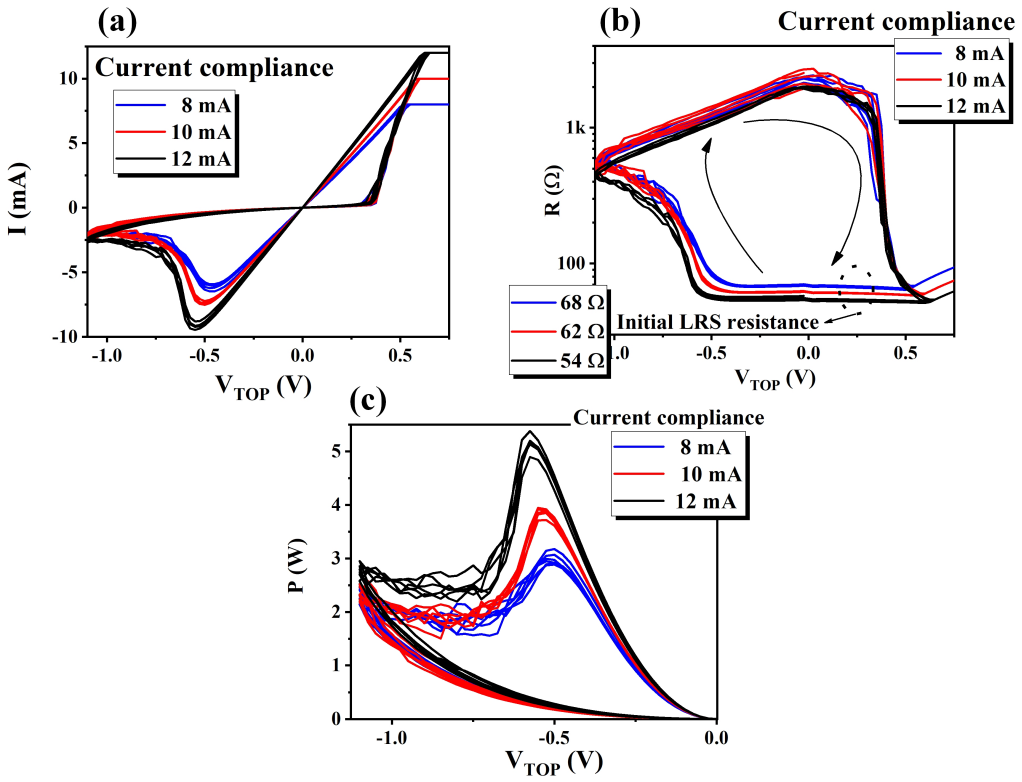

Figure 3: I-V curves using different current compliances: 8, 10 and 12 mA (a), resulting in different R_{LRS}: 68, 62 and 54 Ω, shown in R-V curves (b). P-V curves. Power in the reset transition increases when current compliance increases (c).

is known to be promoted by Joule heating and the electric field [23, 36, 37]. Fig. 4 reveals time to reset differences of about six orders of magnitude (from $\sim$ 0.5 s to $\sim$ 1μs) when the power increases from $\sim$ 4.5 to $\sim$ 13.5 mW, because the power increase implies Joule heating increase. In fact, it is known the effective temperature in the CF can be obtained using the Joule heating formula [38]

$$T = T_0 + R_{Th}P \tag{4}$$

where T is the CF temperature, T_0 is the room temperature, R_{Th} is the thermal resistance and P is the power dissipated by the device. The thermal resistance is defined as the ratio between the maximum temperature increase in the CF and the dissipated electrical power. It is assumed to be proportional to t_{ox}/A, where t_{ox} is the dielectric film thickness and A is the fil-

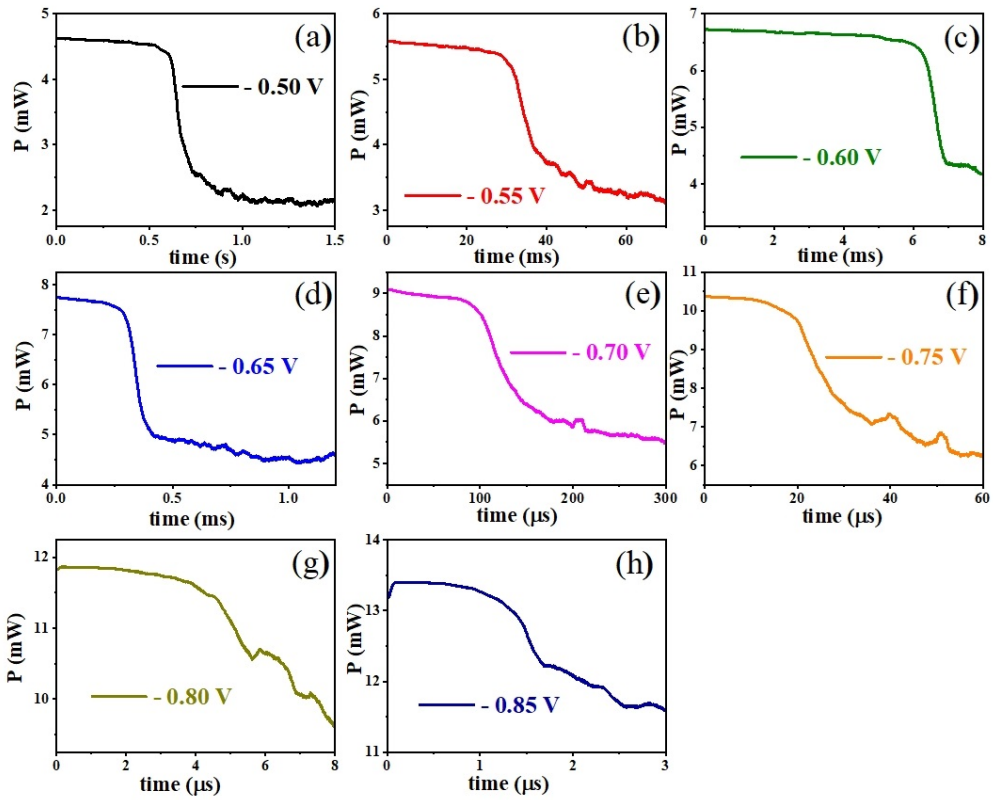

Figure 4: Power transients for the reset transition for an initial R_{LRS}=54 Ω and using a pulse amplitude of -0.50 V (a), -0.55 V (b), -0.60 V (c), -0.65 V (d), -0.70 V (e), -0.75 V (f), -0.80 V (g) and -0.85 V (h).

ament thickness [38, 39]; therefore, the thermal resistance is not only related to the material but also to the filament dimensions. We can assume a similar thermal resistance in all measurements shown in Fig. 4 due to the same initial R_{LRS}, which means the same filament thickness. Moreover, for the CF temperature increase we have not taken into consideration transient effects which can appear in pulse operation. Transient effects have been observed in times shorter than 1 ns in different simulations [38], so we can consider the temperature increase is nearly instantaneous in our measurements.

The higher CF temperature promotes the CF narrowing obtaining lower reset times. The results when the initial R_{LRS} value is 62 and 68 Ω follow the same trend, although the time values are different. Therefore, a strong dependence between the time to reset and the power is observed regardless the initial R_{LRS}.

Fig. 5(a) shows time to reset vs. P for the three initial R_{LRS}. For each power, times increase for lower initial resistances. This corresponds to initial CFs with greater thicknesses. It is clearly a not linear process. The CF dissolution rate is known to be proportional to the ion migration rate [40]

$$\frac{\mathrm{d}\phi}{\mathrm{d}t} = -A \exp\left(\frac{-E_A}{kT}\right) \tag{5}$$

where the CF diameter is ϕ, A is a preexponential constant, k is the Boltzmann constant, T is the CF temperature, and the activation energy is represented as E_A. The CF diameter can be expressed as

$$\phi(t) = \phi_0 - A \exp\left(\frac{-E_A}{kT}\right) t \tag{6}$$

where ϕ_0 is the initial CF diameter. We suppose constant temperature as long as the power dissipated remains constant because transient effects in the heat conduction can be neglected due to the small value of the characteristic thermal time, in the ps range (see [40]).

We can assume time to reset is the time needed to override the CF diameter, so

$$\text{time to reset} = \frac{\phi_0}{A} \exp\left(\frac{E_A}{kT}\right) \tag{7}$$

Taking into account the CF temperature represented in (4), and the activation energy, which is given by [40, 41]

$$E_A = E_{A0} - \alpha q V \tag{8}$$

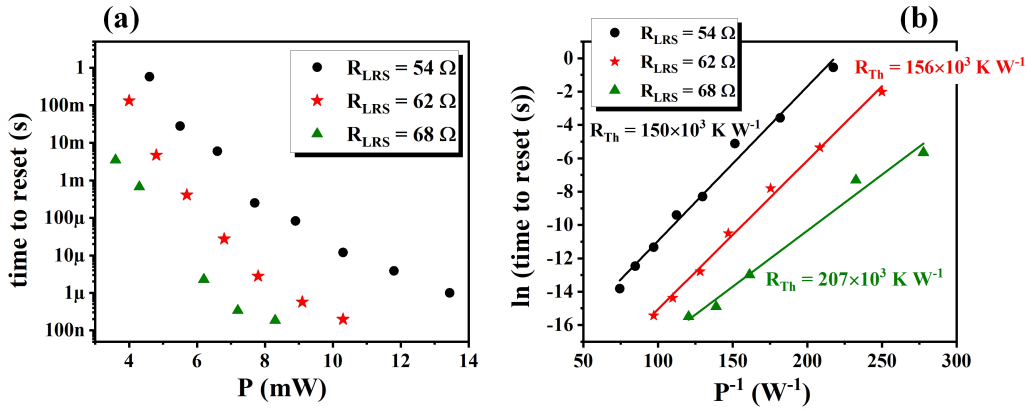

Figure 5: Time to reset vs. power for the different low resistance states (a). Ln(time to reset) vs. P^{-1}. The slope of the linear fit allows us to obtain the thermal resistance value (b).

where the energy barrier for ion hopping is E_{A0}, V is the voltage across the insulating layer, and α is a barrier lowering coefficient, we can represent the time to reset as

$$\text{time to reset} = \frac{\phi_0}{A} \exp\left[\frac{E_{A0} - \alpha q V}{k\,(T_0 + R_{Th} P)}\right] \tag{9}$$

Some simplifications can be made in (9). The filament temperature is much higher than room temperature, so $T = T_0 + R_{Th}P \approx R_{Th}P$. On the other hand, in HfO_x-based memristors, values of E_{A0}=1.2 eV, and α=0.3 are usually used [40], so E_{A0}-αqV $\approx E_{A0}$ for the voltage values used in this work. Using these simplifications, the time to reset can be expressed as

$$\text{time to reset} \approx \frac{\phi_0}{A} \exp\left(\frac{E_{A0}}{k R_{Th} P}\right) \tag{10}$$

Fig. 5(b) shows ln(time to reset) vs. P^{-1} for the three initial R_{LRS}. Taking into account the slope value of the linear fit, the thermal resistance value can be obtained. R_{Th} values depends on the R_{LRS}. It ranges from 150 to 207×10^3 K W^{-1}. Lower R_{LRS} values means thicker conductive filaments so lower thermal resistances, as we have obtained in Fig. 5(b). Values of R_{Th} between 50×10^3 and 500×10^3 K W^{-1} were used in [38] for modeling ReRAM devices.

Finally, in Fig. 6(a) we have represented in a 3D plot ln(time to reset) as function of the initial LRS resistance value and P^{-1}. As we can observe, the points are approximately included in the same plane. The plane equation is

$$\ln(\text{time to reset}) = 10.69 + 0.083P^{-1} - 0.547R_{LRS} \tag{11}$$

To check the accuracy of (11), we have represented in Fig. 6(b), 6(c) and 6(d) the measured times and the times obtained with the plane equation. A good fitting can be observed. This means that we can make a good estimate of the time to reset if we know the initial R_{LRS}, which can be set by applying different current compliances, and the applied power, which can be set from the voltage pulse value. Of course, this equation would not be accurate when transient effects in the heat conduction are not negligible for very fast reset transitions.

4. Conclusions

In this work, we have focused on the reset transition times of HfO_2-based memristors. We have used an electrical characterization setup to obtain the reset transitions when using a constant power signal instead of the conventional voltage constant signal. An initial voltage sweep using different current compliances allows us to obtain different initial low resistivity state resistances, so different initial conductive filament thicknesses. We defined the time to reset parameter as the time it takes for the filament to become thinner before it can be considered broken.

The times for each initial resistance are clearly controlled by the power, which implies different conductive filament temperatures as known by the Joule heating formula. Transition times decreases for higher powers, because the filament temperature is higher, and also decreases for higher initial resistances, because this means a thinner filament. Using the filament dissolution rate, we can obtain the thermal resistance value, an important parameter used in physical simulations of these devices. Thermal resistance values between 150 and 207×10^3 K W^{-1} were obtained, a value compatible with those found in the literature.

Finally, we have observed that the transient times obtained as a function of the initial resistance and the power lies in a same plane. This means we are able to determine the transition time by setting an initial resistance and a power value when the transient effects in the heat conduction can be considered negligible.

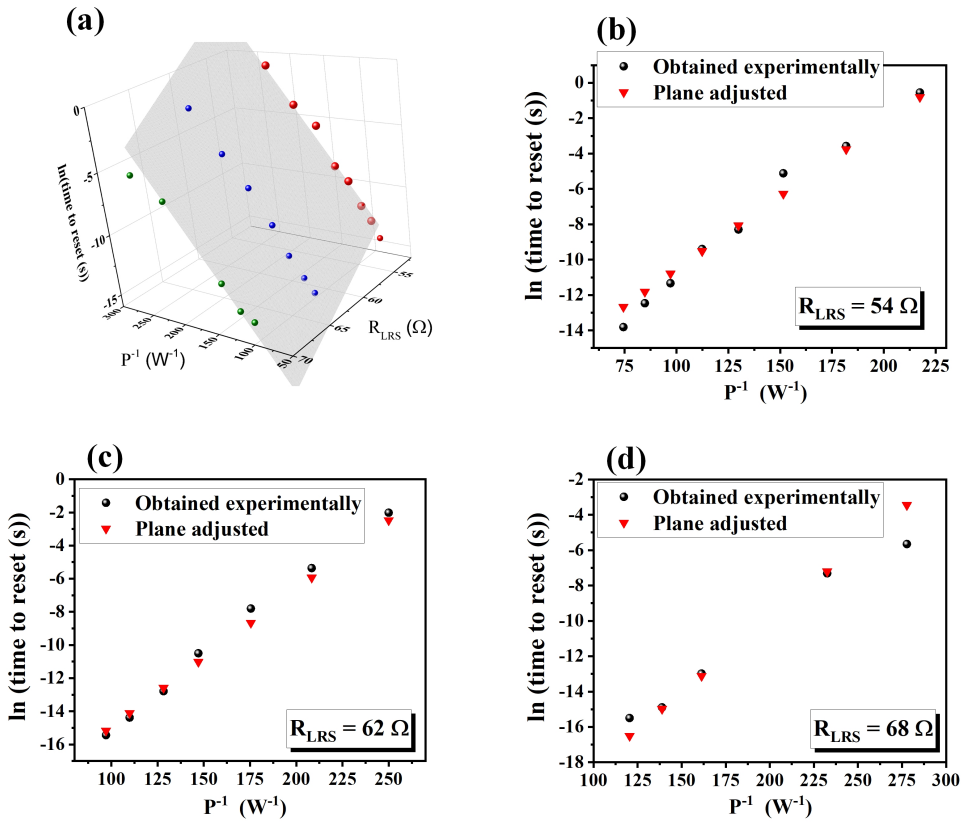

Figure 6: 3D plot of ln(time to reset) vs. R_{LRS} and P^{-1}; all points lie in a plane (a). Comparison of the measured times with the plane equation for different initial resistances, 54 Ω (b), 62 Ω (c) and 68 Ω (d).

Although memristors with lower currents are required for commercial applications, mainly for portable devices, the results obtained in this work can be applied to these devices, as the Joule heating formula and the conductive filament dissolution rate are still valid regardless the filament thickness.

Funding

This work was supported by grants PID2022-139586NB-C43 and PID2022-139586NB-C42 funded by MCIN/AEI/10.13039/501100011033 and by FEDER "A way of making Europe". IMB authors thank the CSIC funding through project 20225AT012, the Generalitat de Catalunya - AGAUR for project 2021 SGR 00497, and the support provided by the project CR32023040125, funded by MICIU/AEI/10.13039/501100011033, and by the European Union through the NextGenerationEU/PRTR program. M.B.G. acknowledges the grant RYC2020-030150-I funded by MICIN/AEI/10.13039/501100011033 and by "ESF Investing in your future" initiative.

References

[1] T. W. Hickmott, Low-Frequency Negative Resistance in thin Anodic Oxide Films, J. Appl. Phys. 33 (1962) 2669–2682, https://doi.org/10.1063/1.1702530.

[2] F. Zahoor, T. Z. Azni Zulkifli, F. A. Khanday, Resistive Random Access Memory (RRAM): an Overview of Materials, Switching Mechanism, Performance, Multilevel Cell (mlc) Storage, Modeling, and Applications, Nanoscale Res. Lett. 15 (2020) 90, https://doi.org/10.1186/s11671-020-03299-9.

[3] M. Lanza, A. Sebastian, W. D. Lu, M. Le Gallo, M-F. Chang, D. Akinwande, F. M. Puglisi, H. M. Alshareef, M. Liu, J. B. Roldan, Memristive technologies for data storage, computation, encryption, and radio-frequency communication, Science 376 (2022) 1066, https://doi.org/10.1126/science.abj9979.

[4] S-O. Park, H. Jeong, J. Park, J. Bae, and S. Choi, Experimental demonstration of highly reliable dynamic memristor for artificial neuron and neuromorphic computing, Nat. Commun. 13 (2022) 2888, https://doi.org/10.1038/s41467-022-30539-6.

[5] W. Zhang, P. Yao, B. Gao, Q. Liu, D. Wu, Q. Zhang, Y. Li, Q. Qin, J. Li Z. Zhu, Y. Cai, D. Wu, J. Tang, H. Qian, Y. Wang, and H. Wu, Edge learning using a fully integrated neuro-inspired memristor chip, Science 381 (2023) 1205–1211, https://doi.org/10.1126/science.ade3483.

[6] I. Vourkas, and G. Ch. Sirakoulis, Emerging Memristor-Based Logic Circuit Design Approaches: A Review, IEEE Circuits Syst. Mag. 16 (2016) 15–30, https://doi.org/10.1109/MCAS.2016.2583673.

[7] Y. Wang, S. Li, Y. Yang, and C. Chen, Progress on Memristor-Based Analog Logic Operation, Electronics 12 (2023) 2486, https://doi.org/10.3390/electronics12112486.

[8] K. S. Woo, J. Han, Si Yi, L. Thomas, H. Park, S. Kumar, and C. S. Hwang, Tunable stochastic memristors for energy-efficient encryption and computing, Nat. Commun. 15 (2024) 3245, https://doi.org/10.1038/s41467-024-47488-x.

[9] R. Dittmann, S. Menzel, and R. Waser, Nanoionic memristive phenomena in metal oxides: the valence change mechanism, Adv. Phys. 70 (2022) 155–349, https://doi.org/10.1080/00018732.2022.2084006.

[10] Z. Fang, X. Peng Wang, J. Sohn, B. Bin Weng, Z. Ping Zhang, Z. Xian Chen, Y. Zhe Tang, G-Q. Lo, J. Provine, S. S. Wong, H.-S. Philip Wong, and D-L. Kwong, The Role of Ti Capping Layer in HfO_x-Based RRAM Devices, IEEE Electron Device Lett. 35 (2014) 912–914, https://doi.org/10.1109/LED.2014.2334311.

[11] M. von Witzleben, S. Wiefels, A. Kindsmüller, P. Stasner, F. Berg, F. Cüppers, S. Hoffmann-Eifert, R. Waser, S. Menzel, and U Böttger, Intrinsic RESET Speed Limit of Valence Change Memories, ACS Appl. Electron. Mater. 3 (2021) 5563–5572,https://doi.org/10.1021/acsaelm.1c00981.

[12] D. Ielmini, Resistive switching memories based on metal oxides: mechanisms, reliability and scaling, Semicond. Sci. Technol. 31 (2016) 063002, https://doi.org/10.1088/0268-1242/31/6/063002.

[13] S. Ambrogio, B. Magyari-Köpe, N. Onofrio, M. M. Islam, D. Duncan, Y. Nishi, and A. Strachan, Modeling resistive switching ma-

terials and devices across scales,J. Electroceram. 39 (2017) 39–60, https://doi.org/10.1007/s10832-017-0093-y.

[14] A. A. Sharma, I. V. Karpov, R. Kotlyar, J. Kwon, M. Skowronski, and J. A. Bain, Dynamic of electroforming in binary metal oxide-based resistive switching memory, J. Appl. Phys. 118 (2015) 114903, https://doi.org/10.1063/1.4930051.

[15] K. Zhang, Y. Ren, P. Ganesh, and Y. Cao, Effect of electrode and oxide properties on the filament kinetics during electroforming in metal-oxide-based memories, npj Comput. Mater. 8 (2022) 76, https://doi.org/10.1038/s41524-022-00770-2.

[16] G. U. Kamble, A. P. Patil, R. K. Kamat, J. H. Kim, and T. D. Dongale, Promising Materials and Synthesis Methods for Resistive Switching Memory Devices: A Status Review, ACS Appl. Electron. Mater. 5 (2023) 2452–2481, https://doi.org/10.1021/acsaelm.3c00062.

[17] D. Kumar, R. Aluguri, U. Chand, and T. Y. Tseng, Metal oxide resistive switching memory: Materials, properties and switching mechanisms, Ceram. Int. 43 (2017) S547–S556, https://doi.org/10.1016/j.ceramint.2017.05.289.

[18] R. Khan, N. Ilyas, M. Z. M. Shamim, M. I. Khan, M. Sohail, N. Rahman, A. Ali Khan, S. N. Khan, and A. Khan, Oxide-based resistive switching-based devices: fabrication, influence parameters and applications,J. Mater. Chem. C 9 (2021) 15755–15788, https://doi.org/10.1039/D1TC03420K.

[19] C. Singh, N. Ray, Memristors and Resistive Switching in Metal Oxides, in: V. Kumar, I. Ayoub, V. Sharma, H. C. Swart (Eds.), Optical Properties of Metal Oxide Nanostructures. Progress in Optical Science and Photonics, vol. 26, Springer, Singapore, 2023, pp. 431-455, https://doi.org/10.1007/978-981-99-5640-1_14.

[20] A. Sawa, Resistive switching in transition metal oxides, Mater. Today 11 (2008) 28–36, https://doi.org/10.1016/S1369-7021(08)70119-6.

[21] S. Brivio, S. Spiga, and D. Ielmini, HfO_2-based resistive switching memory devices for neuromorphic computing, Neuromorph. Comput. Eng. 2 (2022) 042001, https://doi.org/10.1088/2634-4386/ac9012.

[22] Z. Peng, F. Wu, L. Jiang, G. Cao, B. Jiang, G. Cheng, S. Ke, K-C. Chang, L. Li, and C. Ye, HfO_2-Based Memristor as an Artificial Synapse for Neuromorphic Computing with Tri-Layer $HfO_2/BiFeO_3/HfO_2$ Design, Adv. Funct. Mater. 31 (2021) 2107131, https://doi.org/10.1002/adfm.202107131.

[23] S. S. Teja Nibhanupudi, A. Roy, D. Veksler, M. Coupin, K. C. Matthews, M. Disiena, Ansh, J. V. Singh, I. R. Gearba-Dolocan, J. Warner, J. P. Kulkarni, G. Bersuker, and S. K. Banerjee, Ultra-fast switching memristors based on two-dimensional materials, Nat. Commun. 15 (2024) 2334, https://doi.org/10.1038/s41467-024-46372-y.

[24] W. Chen, L. Song, S. Wang, Z. Zhang, G. Wang, G. Hu, and S. Gao, Essential Characteristics of Memristors for Neuromorphic Computing, Adv. Electron. Mater. 9 (2023) 2200833, https://doi.org/10.1002/aelm.202200833.

[25] K. A. Campbell, K. T. Drake, and H. B. Smith, Pulse shape and timing dependence on the spike-timing dependent plasticity response of ion-conducting memristors as synapses, Front. Bioeng. Biotechnol. 4 (2016) 1–11, https://doi.org/10.3389/fbioe.2016.00097.

[26] M. Maestro-Izquierdo, M. B. Gonzalez, F. Campabadal, J. Suñé, and E. Miranda, A new perspective towards the understanding of the frequency-dependent behavior of memristive devices, IEEE Electron Device Lett. 42 (2021) 565–568, https://doi.org/10.1109/LED.2021.3063239.

[27] U. Böttger, M. von Witzleben, V. Havel, K. Fleck, V. Rana, R. Waser, and S. Menzel, Picosecond multilevel resistive switching in tantalum oxide thin films, Sci. Rep. 10 (2020) 16391, https://doi.org/10.1038/s41598-020-73254-2.

[28] E. Yalon, A. A. Sharma, M. Skowronski, J. A. Bain, D. Ritter, and I. V. Karpov, Thermometry of Filamentary RRAM Devices, IEEE Trans. Electron Devices 62 (2015) 2972–2977, https://doi.org/10.1109/TED.2015.2450760.

[29] A. Marchewka, B. Roesgen, K. Skaja, H. Du, C.-L. Jia, J. Mayer, V. Rana, R. Waser, and S. Menzel, Nanoionic Resistive Switching Memories: On the Physical Nature of the Dy-

namic Reset Process, Adv. Electron. Mater. 2 (2016) 1500233, https://doi.org/10.1002/aelm.201500233.

[30] M. Uenuma, Y. Ishikawa, and Y. Uraoka, Joule heating effect in nonpolar and bipolar resistive random access memory, Appl. Phys. Lett. 107 (2015) 073503, https://doi.org/10.1063/1.4928661.

[31] M. von Witzleben, S. Walfort, R. Waser, S. Menzel, and U. Böttger, Determining the Electrical Charging Speed Limit of ReRAM Devices, IEEE J. Electron Devices Soc. 9 (2021) 667–678, https://doi.org/10.1109/JEDS.2021.3095389.

[32] S. Poblador, M. Maestro-Izquierdo, M. Zabala, M. B. Gonzalez, and F. Campabadal, Methodology for the characterization and observation of filamentary spots in HfO_x-based memristor devices, Microelectron. Eng. 223 (2020) 111232,https://doi.org/10.1016/j.mee.2020.111232.

[33] G. González-Cordero, M. B. González, H. García, F. Campabadal, S. Dueñas, H. Castán, F. Jiménez-Molinos, and J. B. Roldán, A physically based model for resistive memories including a detailed temperature and variability description, Microelectron. Eng. 178 (2017) 26–29, https://doi.org/10.1016/j.mee.2017.04.019.

[34] H. García, G. Vinuesa, E. García-Ochoa, F. L. Aguirre, M. B. González, F. Jiménez-Molinos, F. Campabadal, J. B. Roldán, E. Miranda, S. Dueñas, and H. Castán, Effects of the voltage ramp rate on the conduction characteristics of HfO_2-based resistive switching devices, J. Phys. D: Appl. Phys. 56 (2023) 365108, https://doi.org/10.1088/1361-6463/acdae0.

[35] G. González-Cordero, M. Pedro, J. Martin-Martinez, M. B. González, F. Jiménez-Molinos, F. Campabadal, M. Nafría, and J. B. Roldán, Analysis of resistive switching processes in TiN/Ti/HfO_2/W devices to mimic electronic synapses in neuromorphic circuits, Solid State Electron. 157 (2019) 25–33, https://doi.org/10.1016/j.sse.2019.04.001.

[36] X. Zhang, L. Xu, H. Zhang, J. Liu, D. Tan, L. Chen, Z. Ma, and W. Li, Effect of Joule Heating on Resistive Switching Characteristic in AlO_x Cells Made by Thermal Oxidation Formation, Nanoscale Res. Lett. 15 (2020) 11, https://doi.org/10.1186/s11671-019-3229-y.

[37] A. Ascoli, S. Menzel, V. Rana, T. Kempen, I. Messaris, A. S. Demirkol, M. Schulten, A. Siemon, and R. Tetzlaff, A Deep Study of Resistance Switching Phenomena in TaO_x ReRAM Cells: System-Theoretic Dynamic Route Map Analysis and Experimental Verification, Adv. Electron. Mater. 8 2200182, https://doi.org/10.1002/aelm.202200182.

[38] J. B. Roldán, G. González-Cordero, R. Picos, E. Miranda, F. Palumbo, F. Jiménez-Molinos, E. Moreno, D. Maldonado, S. B. Baldomá, M. Moner Al Chawa, C. de Benito, S. G. Stavrinides, J. Suñé, and L. O. Chua, On the Thermal Models for Resistive Random Access Memory Circuit Simulation, Nanomaterials 11 (2021) 1261, https://doi.org/10.3390/nano11051261.

[39] U. Russo, D. Ielmini, C. Cagli, and A. L. Lacaita, Filament Conduction and Reset Mechanism in NiO-Based Resistive-Switching Memory (RRAM) Devices, IEEE Trans.Electron Devices 56 (2009) 186–192, https://doi.org/10.1109/TED.2011.2167513.

[40] D. Ielmini, Modeling the Universal Set/Reset Characteristics of Bipolar RRAM by Field- and Temperature-Driven Filament Growth, IEEE Trans. Electron Devices 58 (2011) 4309–4317, https://doi.org/10.1109/TED.2011.2167513.

[41] R. Meyer, L. Schloss, J. Brewer, R, Lambertson, W. Kinney, J. Sanchez, and D. Rinerson, Modeling the Universal Set/Reset Characteristics of Bipolar RRAM by Field- and Temperature-Driven Filament Growth, IEEE Trans. Electron Devices 58 (2011) 4309–4317, https://doi.org/10.1109/TED.2011.2167513.